

UNCLASSIFIED

AD 414530

DEFENSE DOCUMENTATION CENTER

FOR

SCIENTIFIC AND TECHNICAL INFORMATION

CAMERON STATION, ALEXANDRIA, VIRGINIA



UNCLASSIFIED

NOTICE: When government or other drawings, specifications or other data are used for any purpose other than in connection with a definitely related government procurement operation, the U. S. Government thereby incurs no responsibility, nor any obligation whatsoever; and the fact that the Government may have formulated, furnished, or in any way supplied the said drawings, specifications, or other data is not to be regarded by implication or otherwise as in any manner licensing the holder or any other person or corporation, or conveying any rights or permission to manufacture, use or sell any patented invention that may in any way be related thereto.

AEDC-TDR-63-120



MOLECULAR KINETICS STUDIES

By

**Cord H. Link, Jr.
Scientific Computing Services
ARO, Inc.**

TECHNICAL DOCUMENTARY REPORT NO. AEDC-TDR-63-120

August 1963

AFSC Program Area 850E, Project 7778, Task 7778011

(Prepared under Contract No. AF 40(600)-1000 by ARO, Inc.,
contract operator of AEDC, Arnold Air Force Station, Tenn.)

**ARNOLD ENGINEERING DEVELOPMENT CENTER
AIR FORCE SYSTEMS COMMAND
UNITED STATES AIR FORCE**

414530

**CATALOGED BY DDC
AS AD NO. 414530**

NOTICES

Qualified requesters may obtain copies of this report from ASTIA. Orders will be expedited if placed through the librarian or other staff member designated to request and receive documents from ASTIA.

When Government drawings, specifications or other data are used for any purpose other than in connection with a definitely related Government procurement operation, the United States Government thereby incurs no responsibility nor any obligation whatsoever; and the fact that the Government may have formulated, furnished, or in any way supplied the said drawings, specifications, or other data, is not to be regarded by implication or otherwise as in any manner licensing the holder or any other person or corporation, or conveying any rights or permission to manufacture, use, or sell any patented invention that may in any way be related thereto.

MOLECULAR KINETICS STUDIES

By

Cord H. Link, Jr.

Scientific Computing Services

ARO, Inc.

a subsidiary of Sverdrup and Parcel, Inc.

August 1963

ARO Project No. NW2218

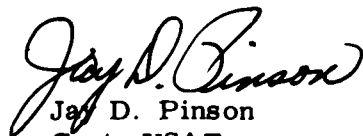
ABSTRACT

A method of calculating molecular flow properties is described, the molecular kinetics (M.K.) method, which is distinctly different from the Monte Carlo method. It has the advantage of permitting the calculation of final asymptotic values directly from initial conditions once the transfer probability matrix for the specific geometry is known. Flow histories may also be developed by a variation of the method.

The general theory is developed, the mathematical operations are described, and applications are shown for selected two- and three-dimensional configurations.

PUBLICATION REVIEW

This report has been reviewed and publication is approved.



Jay D. Pinson
Capt, USAF
Chief, Experimental Division
Space Systems Office



Donald D. Carlson
Lt Col, USAF
Chief, Space Systems Office

CONTENTS

	<u>Page</u>
ABSTRACT	iii
1.0 INTRODUCTION	1
2.0 MONTE CARLO METHOD	2
3.0 MOLECULAR KINETICS METHOD	3
3.1 Calculations	5
3.2 Applications	6
TABLE 1: Matrix Probability for 45-deg Louvre	17
APPENDIX	19

ILLUSTRATIONS

Figure

1. Baffle Geometry	23
2. Reflection Distribution by Zones for Single Zone Input (Louvre)	24
3. Transmission Distribution by Zones for Single Zone Input (Louvre)	25
4. Total Hit Distributions by Zones for Single Zone Input (Louvre), $\theta = 45$ deg	
a. Bottom Wall	26
b. Top Wall	27
5. Reflection by Zones for Directed Beam (Louvre), $\phi = 45$ deg	28
6. Reflection and Transmission of a Directed Beam (Louvre)	
a. Unit Total Beam Strength	29
b. Finite Entrance	30
7. Total Output for Single Input Zone (Louvre), $\theta = 45$ deg	31
8. Typical Configurations and Summary of Results	32
9. Random Angle Geometry for Probability Calculations	33
10. Curves of Constant Transmission	34
11. Simple Masking	35

<u>Figure</u>	<u>Page</u>
12. Masking by Convex Corner	36
13. Schematic of Chevron Configuration	37
14. Probability Equations of Concentric Spheres	38
15. Pulse Propagation between Concentric Spheres . . .	39
16. Zone Geometry, Concentric Spheres	40
17. Molecular Transfers (Target in Northern Hemisphere)	41
18. Types of Transfers	
a. Outer Sphere to Inner Sphere	42
b. Inner Sphere to Outer Sphere	43
c. Outer Sphere to Outer Sphere	44
19. Parallel Beam Geometry for Probability Calculations.	45

1.0 INTRODUCTION

In recent years, with the advent of requirements for space environment simulation, increased attention has been directed to the behavior of low density gas flow both in laboratory experiments and theoretical computations. Especially in the molecular flow regime, computer programs are useful tools for examining interactions between a gas and its physical boundary geometry, the walls of containers and ducts. Two distinct methods are in use.

The first method is the popular Monte Carlo technique in which many individual particles are followed through essentially random processes. Each is traced over a complete history until so many have been traced that statistical inferences may be drawn, extrapolating to the behavior of effectively continuous flow of large numbers of particles.

An alternate method, of prime concern here, develops from radiant energy transfer analysis. For gases in the free molecule regime, analogies may be established between radiant energy flux and particle motion. In this paper we call this method "molecular kinetics" (M. K.). The M. K. method has an advantage of computer speed over the Monte Carlo technique as long as the geometrical boundary configuration is unchanged. The effort required to change configurations is about equal for the two methods.

We shall refer to the Monte Carlo method only for comparison. Both methods share a number of assumptions and have common purposes, that is, to determine certain gross features of gas boundary interactions at low densities.

The following fundamental assumptions are used:

1. All physical surfaces are perfectly diffusing; Lambert's Law holds.
2. No intermolecular collisions occur.
3. An ergodic hypothesis for equilibrium holds: the time average velocity of one molecule is equivalent to the instantaneous average velocity of a large number of molecules so that a single velocity suffices to characterize the system.

Similar assumptions occur in much radiant heat-transfer theory, incorporated in assumptions such as diffuse reflection and emission, isotropic non-dispersive media, and the use of geometrical optics.

Manuscript received May 1963.

2.0 MONTE CARLO METHOD

A geometrical boundary configuration is described, initial starting locations (sources) are established by some selection rule, and the line of motion of a particle is found by pseudo-random methods based on a statistical distribution model such as Lambert's Law. The equation of the line of motion is solved simultaneously with equations of target surfaces to find the first intersection. This point is treated as a new origin, and a new path line is generated. The tracing stops when some final conditions are met, such as "loss" of the particle back to the source or "capture" by a sink. Then a new particle is generated at the source.

After large numbers of particles have been traced, one may, with caution, begin to draw statistical inferences about the behavior of effectively continuous streams of particles. This method may be thought of as a combination of discrete particles with piecewise continuous geometry of the boundary. The molecular kinetics method, in contrast, may be thought of as a combination of continuous flow with discrete segmented geometry. Both methods are practical approximations to the real problem in which both boundary and flow are in some sense continuous; solutions are usually not available for this problem.

2.1 ERRORS

The precision of the Monte Carlo technique is inherently limited only by time if care is taken to reduce the possibility of systematic bias. The M. K. method is limited in precision by the fundamental assumption of uniform density over each increment of area at each step. The error is at its worst for concave corners but can be reduced by adopting non-uniform area increments to improve the approximations where the densities are changing most rapidly with position.

2.2 COMPUTING PROBLEMS

The Monte Carlo method requires time principally from the need for large numbers of runs so that statistical averages have validity. The randomness of the process is never overcome completely. The computer program acquires bulk when the boundary of the system is to any degree complex, and it requires sophisticated programming to avoid long searching for intercepts of lines of motion with the boundary.

3.0 MOLECULAR KINETICS METHOD

The geometry is subdivided into discrete elements for all pairs of which "angle factors" (influence or form factors) may be calculated. * These factors have the property that for any source elements facing a closed boundary of surface elements, all factors sum to unity. They are also by definition a distribution function; they give the fraction of radiation leaving the source element and intercepted by each of the target elements. They may thus be interpreted as transfer probabilities, giving the probability that a particle from a source element will strike a target element. Finally, they are functions of relative orientation between two elements, hence functions of location of both. We shall use the name "transfer probability" for "angle factor".

The geometrical segments, or zones, may be labeled in order; thus Z_i is the i th zone with i ranging from 1 to N , a finite but often large number. Then P_{ij} will represent the probability of transfer from zone i to zone j . By definition of P_{ij} we have

$$\sum_{j=1}^N P_{ij} = 1 \quad (1)$$

i. e. , all particles leaving arrive somewhere. The P_{ij} may be conveniently thought of as a square matrix of size $n \times n$. We shall use the probability matrix to distribute particles from source elements i to target elements j . We start with a given initial distribution of particles in one or more zones. Since there are N zones, we may think of the original particle distributions in source zones as the N components of a vector, $V_i(0)$, $i = 1, 2, \dots, N$. At least one $V_i(0)$ is non-zero. By this approach we easily describe any original particle distribution in any pattern over the geometric elements.

We have implicitly introduced one source of error by the tacit assumption that the distribution of particles within a zone is either uniform or has some assignable mean location. It is plain that any distribution can be approximated as closely as we wish by making N sufficiently large so that the area elements approach infinitesimal size.

The original distribution $V_i(0)$ is transferred as a pulse to all target zones by the simple process to produce the next distribution,

$$V_j^{(1)} = \sum_{i=1}^N P_{ij} V_i^{(0)} \quad (2)$$

*Jakob. Heat Transfer. Vol. 2, Chapter 31, John Wiley, New York.

We must now invoke the assumption that the particles arriving at the target zone are uniformly distributed over that zone if we are to proceed.

We introduce now a reflection coefficient, having a value between zero and unity and dependent on that zone, which we label A_i . If $A_i = 1$, the zone absorbs no particles, but if $A_i = 0$, it absorbs all the incident particles. By this means, we may have porous walls or may introduce holes in the boundary. Any zone, i , for which $A_i = 0$, is a hole from which incident particles do not return.

We may now calculate one step further. The distribution remaining after the first transfer (Eq. (2)) may be modified by the reflection coefficient so that the resulting distribution

$$A_j V_j^{(1)} = A_j \sum_{i=1}^N P_{ij} V_i^{(0)} \quad (3)$$

remains to be transferred by the process

$$V_j^{(2)} = \sum_{i=1}^N P_{ij} A_i V_i^{(1)} \quad (4)$$

The repeated application of the above steps is called the "bounce" approach and may be continued indefinitely. If any A_i are less than unity, the original particles will eventually all leak out, all components $V_i^{(M)}$ becoming vanishingly small, and the process is usually terminated when the sum (or largest) of the $V_i^{(M)}$ becomes insignificant relative to the original total distribution

$$\sum_{i=1}^N V_i^{(0)}$$

Several quantities of interest may be developed. Suppose that zone K is a hole; that is, $A_K = 0$. Then the leakage through zone K at bounce M is $V_K^{(M)}$. This quantity may be summed for all bounces to give the total transmission through the hole, which may be one of many or part of a larger hole, so that we may obtain transmission through the hole as a distribution over its parts.

Quantities so developed approach asymptotic values which may be obtained directly. It is accepted that an infinite sum over a history of one original distribution is equivalent to a sum of current contributions of an infinity of like distributions originating uniformly in the past. This assumption allows direct development of asymptotic values and implies a steady state of flow.

3.1 CALCULATIONS

3.1.1 Asymptotic Calculations

We modify notation slightly so that V_0 represents our original distribution vector, P is the matrix of elements (P_{ij}) , and A is a diagonal matrix of reflection coefficients (A_{ii}) . We define the "hit" vector H for molecules, incident on the zones as follows: subscripts denote "bounce" number. P' is the transpose of P .

$$\begin{aligned} H_1 &= P' V_0 & A H_1 &= V_1 \\ H_2 &= P' A H_1 & A H_2 &= V_2 \\ H_3 &= P' A H_2 & & \vdots \\ &\vdots & & \vdots \end{aligned}$$

Summing over all bounces for $H_T = H_1 + H_2 + H_3 + \dots$

$$I H_T = P' V_0 + P' A H_T$$

where I is the identity matrix and by rearrangement,

$$(I - P' A) H_T = P' V_0$$

Hence

$$H_T = (I - P' A)^{-1} (P' V_0) \quad (5)$$

for the asymptotic value of total hits. H_T is a vector, and its components are total hits per zone.

If we define F as the flux of particles from a zone, we have in the same way

$$\begin{aligned} F_0 &= V_0 \\ F_1 &= A P' V_0 \\ F_2 &= A P' F_1, \dots \end{aligned}$$

or

$$I \cdot F_T = A P' F_T + V_0 + A P' V_0 \quad (6)$$

thus

$$F_T = (I - A P')^{-1} (V_0 + A P' V_0)$$

The hit vector H is related to pressure distributions, flux vector F is related to the density in the space near the boundary within the system, and their difference $(H-F)$ is related to the leakage out of the system (i. e., pumping loads). These quantities are vectors whose elements associate with their corresponding zones.

3.1.2 Computing Problems

In the molecular kinetic approach, all geometry interactions are incorporated into the transfer probabilities. Herein lies the bulk of computing time. These probabilities are not always simple to compute, as will be brought out in later applications. But once computed for a given configuration, the probability matrix need not be repeated. There remains the problem of computer memory size since the P matrix is to be stored, and for asymptotic cases, room must be allowed for the matrix inversion and storage. Thus, the fineness of geometry subdivision is controlled primarily by computer storage. This problem is partly solved by block programming, logical blocks being (1) probability calculations, (2) preparation of matrix for inversion, (3) matrix inversion, and (4) final calculations (probability calculations or "bounce" transfer calculations repeated).

Block programs along these lines have been prepared for limited general cases with only step (1) needed for specific applications. In addition, other programs have been prepared to take advantage of symmetry problems and matrix partitioning when these can be utilized in special applications.

For some configurations, we have in the molecular kinetics method a much faster program than the Monte Carlo approach will allow. In the following sections we will indicate how an M. K. program can provide information to improve "convergence" of a Monte Carlo program.

3.2 APPLICATIONS

3.2.1 Two-Dimensional Applications

3.2.1.1 Two-Dimensional Models

Many configurations of interest may be described approximately by general cylindrical surfaces generated by a family of parallel straight lines of infinite length. An infinitely long strip of infinitesimal width characterizes a surface element. If all surface elements are of this kind, then the probabilities for particle transfer are independent of location along the length of the source strip, and an integration may be performed along the target strip to obtain probability of transfer from source strip to target strip. The configuration may be represented by any cross section perpendicular to the generating lines. The cross-section plane representation of cylindrical surfaces is what is usually meant by a two-dimensional model.

Typical of current uses of Monte Carlo and M. K. programs are calculations related to the baffle configurations used with cryopump panels. These low temperature pumping surfaces have low heat conduction, and it is desirable that molecules arriving at the cryosurface should be of low energy. This is accomplished by insuring that a large part of the molecules have lost energy by collisions with low temperature (but not pumping) baffle surfaces before they arrive at the cryopump. One seeks a configuration which can be cheaply fabricated but has good efficiency in effecting energy loss from the molecules while passing on enough molecules for the cryopumps to function at reasonable speeds without overheating.

Of course, the real baffles are three-dimensional, but they are generally of plane strip elements so that except for their finite length and their ends, they may be treated in section (i. e., as two-dimensional systems) provided their length is large relative to their other dimensions. To precisely account for end surfaces requires a three-dimensional approach. Since results are available in the literature for Monte Carlo runs for two-dimensional baffle geometry, the M. K. system can be compared to Monte Carlo results for specific cases.

We shall go into some detail for the configuration of slanted parallel plates known as "louvres" and their back-to-back arrangement called "chevrons" and examine their behavior by the molecular kinetics method.

The louvres considered are optically tight for normal incidence; the chevrons are opaque for any incidence angle (Fig. 1).

For the detailed study of the louvre, all faces (entrance to left, exit to right) were divided into eight equal zones, and the resulting 32 by 32 probability table was computed (Table 1). We obtained the asymptotic hit vector for input on each separate zone of the entrance face when the entrance and exit faces have zero reflection coefficient and all other faces have unity (perfectly absorbing ends, perfectly diffusing-reflecting walls).

It is plain that the reflectivity of the configuration is the ratio of the total hits absorbed by the entrance face to the total input. Also the net transmissivity is the total of hits absorbed on the exit face. Recall that total hits are available for each zone. We may then plot the reflectivity and transmissivity of the configuration as a function of position on the input face. Our specific case has $\theta = 45$ deg.

Figure 2 shows the distribution of reflected particles for each single input zone; Fig. 3 shows the transmission distribution. These are quite

sensitive to location of input; consequently, we deduce that the Monte Carlo solution to this problem would be very sensitive to any bias of input points. For completeness, we show the total hit distribution on the louvre walls (Fig. 4a and b) which correspond to pressure distributions.

These results are for perfectly random flow incident from the left. Since by means of the original distribution vector we can place the initial distribution wherever we please, and we examine the results for directed streams. Part or all of such streams are started on the louvre walls. The dependence of reflection and transmission on stream direction is shown in Fig. 5, distributed over the output (entrance) faces for reflection.

Figure 6a shows the reflection-transmission properties for the 45-deg louvre as a whole and as a function of input direction. In Fig. 6b, this has been properly weighted to account for the finite entrance (cosine biased).

Finally, Fig. 7 shows the net reflection-transmission properties for the louvre as a function of input position in random flow with the final, lumped values marked under uniformly random input. This shows that for this configuration a "flat" distribution of locations on the entrance face in a Monte Carlo run could be replaced by a single "mean" entry point, almost at the middle of the entrance face. For the Monte Carlo method, this would remove one random variable from the process, thereby speeding the convergence of the process.

Figure 8 is a summary of results for several louvre angles and a parallel plate.

3.2.1.2 Two-Dimensional Transfer Probabilities

We define a source zone as a line segment extending from $y_1 = 0$ to $y_1 = A$ at $x_1 = 0$. It has an aperture height A . We will find the probability for perfectly random-oriented and positioned paths from the left of the aperture ($x < 0$) to pass through the aperture and above a point (x_2, y_2) to its right (Fig. 9).

We evaluate the integral for the fraction passing above the point (x_2, y_2)

$$T_{A, (\bar{2})} = \frac{1}{2A} \int_{y_1=0}^A \left[\int_{(2)}^{\infty} \frac{\cos \phi_1 \cos \phi_2}{r_{12}} dS_2 \right] dy_1 \quad (7)$$

Since we require only the region above the point (x_2, y_2) we may, for the inner integral, substitute integration along a circular arc from ϕ_{\min} to $\pi/2$, on which $\cos \phi_2 = 1$ and $dS_2/r_{12} = d\phi_1$.

$$\begin{aligned}
T_{A, (\bar{2})} &= \frac{1}{2A} \int_0^A \left[\int_{\phi_{\min}}^{\pi/2} \cos \phi_1 d\phi_1 \right] dy_1 \\
&= \frac{1}{2A} \int_0^A (1 - \sin \phi_{\min}) dy_1
\end{aligned} \tag{8}$$

By construction $\sin \phi_{\min} = \frac{y_2 - y_1}{\sqrt{x_2^2 + (y_2 - y_1)^2}}$
hence

$$\begin{aligned}
T_{A, (\bar{2})} &= \frac{1}{2A} \left[y_1 - \sqrt{x_2^2 + (y_2 - y_1)^2} \right]_{y_1=0}^A \\
&= \frac{1}{2A} \left[A - \sqrt{x_2^2 + (y_2 - A)^2} + \sqrt{x_2^2 + y_2^2} \right]
\end{aligned} \tag{9}$$

In particular if A is taken as unity (if x, y are scaled to the unit A)

$$T_{1, (\bar{2})} = \frac{1}{2} \left[1 - \sqrt{x_2^2 + (y_2 - 1)^2} + \sqrt{x_2^2 + y_2^2} \right] \tag{10}$$

By noting that the radicals are simply distances between (x_2, y_2) and respectively, $(0, A)$ and $(0, 0)$, we can use distances between points

$$T_{A, (\bar{2})} = \frac{1}{2} \left[\frac{r_{0A} - r_{A2} + r_{02}}{r_{0A}} \right] \tag{11}$$

(See Fig. 9c.)

Since r_{0A} is the aperture A, constant, we can establish that lines of constant $T_{A, (\bar{2})}$ occur for points (x_2, y_2) satisfying

$$r_{02} - r_{A2} = \text{constant} \tag{12}$$

and such lines of constant $T_{A, (\bar{2})}$ are a family of confocal hyperbolae, with foci at $(0, 0)$ and $(0, A)$. A graph of constant T lines has some utility, as will be shown.

Suppose now that we introduce another point (x_3, y_3) and calculate

$$T_{A, (\bar{3})} = \frac{1}{2} \left[\frac{r_{0A} - r_{A2} + r_{02}}{r_{0A}} \right] \tag{13}$$

Provided only that the entire new line segment r_{23} is visible from all of r_{0A} , it is plain that the probability of random rays through r_{0A} striking the line r_{23} is just

$$\begin{aligned}
P_{0A, 23} &= |T_{A, (\bar{3})} - T_{A, (\bar{2})}| \\
&= \frac{1}{2} \left| \frac{(r_{A2} - r_{02}) - (r_{A3} - r_{03})}{r_{0A}} \right|
\end{aligned} \tag{14}$$

where the absolute value is indicated to ensure a positive (meaningful) result, independent of which direction on r_{23} is taken to be positive.

This formulation, incidentally, is now independent of position and orientation of the figure since only displacements between points are involved.

The confocal hyperbola graph can now be used to evaluate transfer probabilities between two line elements by constructing the elements to scale. A single graph for $A = 1$ is sufficient provided all distances are converted to units of A (Fig. 10).

It is now possible to calculate transfer probabilities for any configuration of line elements in the plane so long as they are all completely concave to one another. That is, each one must be entirely visible from all points of any other element. This condition is obviously satisfied for any parallel line segments, hence for the louvre configuration.

However, it is necessarily assumed in this development that a source segment is perfectly randomly filled with transfer rays, hence, uniformly filled. It is also plain that, after transfer of molecules from source to target arrays, the distributions on the targets will be non-uniform. This dichotomy can be resolved, in part, only by taking sufficiently small line segments, even for linear arrays. By this means, the discrepancy in assumed distributions and accurate (continuously varying) distributions may be made as small as we please.

Referring again to the loci of constant $T_{A, (2)}$, some of their properties are of interest. The slope of the hyperbola at point $(x_2 y_2)$ can be easily found to be that of the bisector of the angle included between the lines r_{02} and r_{A2} . As the point $(x_2 y_2)$ is removed to remote distances, such that r_{0A} becomes of differential size relative to r_{12} , the hyperbola of constant $T_{A, (2)}$ approaches asymptotically the line from the midpoint of aperture A , inclined at angle ϕ_∞ , appearing in

$$T_{A, (\phi_\infty)} = \frac{1}{2} [1 - \sin \phi_\infty] \quad (15)$$

This relation is useful in estimates of probabilities at large distances.

For transfer to a line segment r_{23} at great distances

$$P_{A, (r_{23})_\infty} = \frac{1}{2} |\sin \phi_1 - \sin \phi_2| \quad (16)$$

a form which is well known as the plane "angle factor" from a differential line segment to any arc between angles ϕ_2 and ϕ_3 or for a differential area

to a general cylinder whose generating lines are parallel to the differential area bounded by angles ϕ_2 , ϕ_3 relative to the normal to the differential area.

3.2.1.3 Transfer Probabilities with Masking

The louvre probabilities are quite simply evaluated since all line elements are strictly concave relative to one another. When there exists convexity in the figure, it is necessary to modify the procedure to some extent. We examine the meaning of the terms convexity and concavity.

Suppose line elements (A, B) and (C, D) are so oriented that (A, B) extended intersects between (C, D). (See Fig. 11.) The plainly the two "sides" of a (A, B) "see" separate parts of (C, D). We must then clearly indicate which faces are the front faces and assign zero probabilities for relative orientations which involve back faces. The point of intersection is labeled E, and E is an end point for a smaller segment which may be used to compute the probability (see Fig. 14).

This is the simplest form of masking where one line element effectively casts a shadow on another, reducing its transmission to the other. If the intersection E lies on the source element, a fraction f of the source sees the front face of the target. By the assumed uniform distribution within an element, f enters as a multiplier of the probability computed for the fractional part of the source that does not see the target. However, if the point E lies in the target, the probability is computed from source to that part of the target in view from the front of the source. These two quantities differ in that for E in the source, only part of the source "radiation" can be transmitted, whereas with E in the target, all of the source radiation is transmissible to part of the target.

A more complex form of masking occurs when a convex part (Fig. 12) of the boundary is interposed between source and target. Let the end of the mask point be labeled M. Then lines from A, B, C, or D through M will cross within the elements (A, B) or (C, D) if masking occurs.

Consider the configuration shown where (A', B') is the segment of (A, B) where masking occurs. We see that (A, A') does not see (C, D) at all, but that (B', B) sees all of (C, D). Thus, (B', B) and (C, D) may be simply inter-related as a simple concave pair.

It is plain that any rays drawn from (A', B') to (C, D) must pass through the line (M, D). Thus we may use (A', B') and (M, D) as a simple concave pair to obtain the probability from (A', B') to (C, D). Likewise, all rays from (C, D) to (A, B') must pass through (M, B'). So the probability

for (C, D) to (A, B') is computed from the simple concave pair, (C, D) to (M, B'). To this is added the contribution of (C, D) to (B, B'). This situation is summarized in Fig. 12.

More complicated masking can occur in some configurations such as two or more points like M. They may all be handled by arguments similar to these, breaking the segments into more simply related parts.

We are now in position to compute all transfer probabilities for the chevron configuration, as illustrated in Fig. 13. We use Roman numerals to distinguish the six major faces and use a symmetrical numbering scheme for the six N faces, N being the number of segments in each face. (It is, of course, not necessary to use either equal size segments or equal numbers of segments per face.)

We see that probabilities between faces I, II, and III are already obtained in the louvre case. (By symmetry, whatever we say of faces I, II, and III holds for IV, V, and VI.) Also the upper half of face IV is simply concave toward I, II, and III, while V and VI are not visible from I and II. Part of III sees IV, V, and VI, but the relations between I, IV, and VI (for lower III) involve masking by the junction of II and V. We note also that the first type of masking discussed can occur for II, IV transfers, but this is removable by making the point of intersection of II (extended) with IV, a point of division segments of IV. For $\theta = 45$ deg, we provide this by requiring an even number of segments per face.

3.2.1.4 Criticism of Louvre and Chevron Results

By comparison with results of other workers using Monte Carlo or laboratory methods, the present transmission factors are usually a few percent high. This is a direct consequence of the assumed uniformity of distribution of flux on the target zone, an assumption which is in reality violated at any concave corner. In effect, the original flux is inserted somewhat deeper into the figure than intended.

The following illustrates the point. Suppose we had two adjacent segments at right angles. We find $P = 0.283$ as the transfer probability. Now reduce segment size by one half, and the probability is unchanged. Thus, at the corner, if the segment is $1/n$ of the original segment, then $0.283/n$ of the original flux is transferred at the corner, and less, elsewhere. The corner is a "hot spot" with highest concentration. Now the assumption of uniformity in a target zone plainly causes an effective shift of the flux away from the corner.

This error, commonly found in radiant heat-transfer numerical calculations, can be reduced only by finer subdivision, particularly at corners but generally in regions where the transfer probability changes most rapidly with location. By this means, not only are the distributions shifted a lesser amount, but the number of zones causing significant error is relatively reduced.

3.2.2 Three-Dimensional Applications

3.2.2.1 Geometry

The problem of concentric spheres constituted our introduction to the M. K. method, a problem specially formulated for its application from which we have generalized the method to other configurations.

The investigation involved developing a concept of "pressure" in molecular flow, in particular for a spherical space environment simulator. An inner concentric sphere was an idealized space vehicle. The gas flow space was thus completely bounded between the outer "chamber" and the inner "vehicle".

The problem was formulated by C. Tsonis of General Electric Company (under contract AF 40(600)-954) with computing support provided by ARO, Inc., Arnold Engineering Development Center. * Tsonis used the distinction between the concave chamber and the convex vehicle to separate the transfer probabilities into three parts (effectively partitioning the probability matrix) and invoked the symmetry of the system to reduce the calculating effort. Most significant of all, Tsonis integrated the integral expressions for transfer probabilities to provide closed forms for direct numerical calculations.

As originally proposed, our problem was simply to program the expressions provided. It was intended that the spheres be divided into $2N$ coaxial spherical zones, where N was a "large" number, nominally 20 to 40. Since three kinds of transfer occur, this means we had to provide storage for three 80 by 80 arrays, in effect. Equatorial symmetry of geometry reduced this to three 40 by 80 arrays, and a simple relation between two of these resulted in only two 40 by 80 arrays being required. This made the program tractable for use with our computer (IBM 7070, 10K storage). The program was blocked to compute probabilities first, then to compute the flow characteristics with another program.

*C. A. Tsonis, "Molecular Flux Distribution in an Aerospace Chamber - Analysis of Gas Kinetics - Summary Report," AEDC-TDR-63-88, April 1963.

The "bounce" technique was first utilized with control option for the number of bounces. Later, the same problem was proposed to be done in terms of matrix algebra to arrive directly at asymptotic values. For the matrix method, the requirement of computing speed and the necessity for more arrays in storage led to reducing the program capability so that the maximum array was 40 by 40, which proved adequate. In every case so far tried, the matrix (40 by 40 maximum) to be inverted was so well conditioned that single precision matrix inversion (by diagonalizing) was adequate.

The equations programmed are included in this paper (Fig. 14) together with a special demonstration of pulse propagation through a small space between a chamber and a vehicle that nearly fills the chamber (Fig. 15).

For plane surface boundaries and for some simple shapes in various relative positions, the transfer probabilities may be calculated from the formulae in the literature. More generally, one can expect the necessity of developing numerical values from the fundamental integral definition.

$$P_{\Delta A_1, \Delta A_2} = \frac{1}{\Delta A_1} \int_{\Delta A_1} \int_{\Delta A_2} \frac{\cos \phi_1 \cos \phi_2 d\Delta A_1 d\Delta A_2}{\pi r_{12}^3}$$

It is quite possible to numerically integrate this quadruple integral; the integration limits often cause considerable difficulty.

It should be noted that integration can also be done by the Monte Carlo method by estimating the fraction of starts from the source that will strike the target segment somewhere. This is quite feasible since only single step processes are involved, not long process chains.

We will devote attention to the concentric sphere case. For axisymmetric geometry with constant latitude zone boundaries, the probability integrals were evaluated by Tsonis and are given in Fig. 14.

3.2.2.2 Transfer Equations

The relative size of two concentric spheres is completely defined by the relation $r_{\text{inner}} / r_{\text{outer}} = \sin \gamma$. We chose a polar coordinate system with a common polar axis. Let each sphere be divided into $2N$ zones whose boundaries are plane circles parallel to the equatorial plane, defined by constant angle θ from the equator and having uniform angular width $\Delta \theta = \pi / 2N$.

A zone is associated with its lower boundary, and its zone index numbers (I for source zone, J for target zone) start at the south pole, $\theta = -\pi/2$. Theta (θ) is the latitude angle.

We assume axial symmetry so that our expressions hold uniformly in longitude. Hence the probability of a molecular transfer from zone I to zone J depends solely on θ_I , θ_J , $\Delta\theta$, and γ .

In obtaining the transfer probabilities, transfers from zone θ_I to the entire region above θ_J are calculated:

$$P(\theta_I, \theta \geq \theta_J)$$

and

$$P(\theta_I, \theta \geq \theta_{J+1})$$

(Fig. 16).

then

$$P(\theta_I, \theta_J) = P(\theta_I, \theta \geq \theta_J) - P(\theta_I, \theta \geq \theta_{J+1})$$

for all θ_I but for only $0 \leq \theta_J < \pi/2$. By equatorial symmetry the remaining values are assigned since the symmetry means that

$$P(\theta_I, \theta_J) = P(\theta_{2N-I+1}, \theta_{2N-J+1})$$

when I and J range from 1 to 2N.

There are three types of transfers (Fig. 17): outer sphere to inner sphere (1), inner sphere to outer sphere (2), and outer sphere to outer sphere (3). The type inner to inner does not occur since the inner sphere is totally convex to itself. In all types of transfers we limit the calculation to transfers from any source location to "caps" above the equator by reason of equatorial symmetry.

In the outer sphere to inner sphere transfers (1), no part of the upper hemisphere is visible from latitudes below $\theta_I = \pi/2 - \gamma$. The part of the inner sphere visible from a point at $\theta_I > \pi/2 - \gamma$ is the region in common with the cap (θ_J) and the cone of half vertex angle γ . This is described by Eq. (2) of Fig. 14 until $\theta_I \geq \gamma$. When this point occurs, some caps (θ_J) lie wholly within the γ cone of the point at θ_I , and these wholly contained caps have probabilities calculated from Eq. (1) of Fig. 14 (Fig. 18a).

In the inner sphere to outer sphere transfers (2), the bounding curves are the cap (θ_J) lower boundaries and the horizon circle on the outer sphere, cut by the plane that is tangent to the point (θ_I) on the inner sphere. The same limits on θ_I apply as for type (2) transfers. Near the south pole, there is a range of θ_I for which the horizon circle does not project above the equator. Then there is a range such that the horizon circle cuts caps in the northern hemisphere so that the cap boundary and the horizon circle together define the region to which transfer may occur, and Eq. (4) of Fig. 14 is used. Finally, some caps occur wholly contained within the

horizon circle, and these have probabilities calculated from Eq. (3) of (Figs. 18b and 14).

In the outer sphere to outer sphere transfers (3), the main boundary feature is the shadow of the inner sphere cast on the outer sphere (Figs. 18c and 14).

If the shadow is wholly below the spherical cap (θ_J), the probability is given by Eq. (5). If this shadow cuts the spherical cap (θ_J) then Eq. (7) is used. But if the shadow is wholly contained within the cap (θ_J), Eq. (6) is used.

In the cases computed, γ was taken to be some multiple, N_2 , of $\Delta\theta$, so that all tests concerning which equation to use are based on relations between zone index numbers I and J and the numbers N_2 and N. It is well to note that Eqs. (1) and (2) differ from Eqs. (3) and (4) only by a factor $\sin^2 \gamma$; the computer programs take advantage of this as well as symmetry to minimize storage problems.

3.2.2.3 Example of Results Obtained

We show (Fig. 15) a plot of results using the bounce system to describe the propagation of a pulse of molecules originating on the zones on either side of the equator. The same input is started on both spheres, and the result is a wave propagating toward the poles. A reflection coefficient of unity preserves all the molecular flux. It is apparent that the pulse is diffusing as well as moving away; after several hundred bounces the gas would be practically uniformly distributed.

For further applications see Tsonis (AEDC-TDR-63-88).

TABLE 1
PROBABILITY MATRIX FOR 45-DEG LOUVRE

[illegible]

APPENDIX

THE "COSINE BIAS" LAW

Let us imagine a space in which particles have completely random positions and directions of motion. If we now introduce a plane imaginary surface into this space and examine the passage of particles through the surface, we see the controlling factor is the projected area of the surface. The maximum number of paths through the surface is associated with directions normal to the surface, and minimum, for directions parallel to it. The projection of an area in a given direction invokes the cosine of the angle between that direction and the normal to the area. This is the purely geometrical origin of the cosine bias law.

To see that this law holds in two-dimensional geometry, it suffices to observe that completely random directions in three dimensions project onto any plane as equally random directions and that the projection of a line segment in a given direction still involves a cosine factor.

In either case, in writing a cosine bias distribution for directional probabilities, it is mandatory to normalize the distribution so that the integral of the distribution over all realizable directions is unity.

We note that the above discussion is independent of rates of motion, i. e., of velocity, and the cosine bias law does not incorporate any increase of "forward" scattering at very oblique incidence.

ALTERNATE PLANE PROBABILITY CALCULATION

We will develop here an alternative approach to calculating transfer probabilities in the plane. We will find the average fraction of parallel streams from a source aperture to the region above a given point, averaging over all orientations of the stream.

As before, the source is a line segment on the y-axis, $0 \leq y \leq A$. A point (x, y) is to the right. The source is illuminated from the left with a strictly parallel beam inclined at angle ϕ to the x-axis. The beam at least fills the source aperture (Fig. 19).

The point (x, y) may be in or out of the beam issuing from the source. We calculate the fraction $f(\phi, x, y)$ of the beam passing above (x, y). The width of beam through (0, A) is $A \cos \phi$.

Plainly, for general finite (x, y) anywhere to the right of $(0, A)$, there is some range of ϕ for which no part of the beam passes above (x, y) ; this is the range $-(\pi/2) < \phi < \phi_{\min}(x, y, A)$. Also there is some range for which the entire beam passes above (x, y) ; this is the range $\phi_{\max}(x, y, 0) < \phi < (\pi/2)$. And finally, over the range $\phi_{\min} < \phi < \phi_{\max}$, some fraction of the beam passes above (x, y) .

We define the two distances

$$r_a(x, y, A) = \sqrt{x^2 + (y - A)^2}$$

$$r_o(x, y, 0) = \sqrt{x^2 + y^2}$$

and from the figure, find the beam width

$$A \cos \phi = r_o \sin(\phi_{\max} - \phi) + r_A \sin(\phi - \phi_{\min})$$

and the fraction of beam passing above (x, y) is thus

$$\left. \begin{aligned} f &= 0 \\ f &= (r_A \sin(\phi - \phi_{\min})) / A \cos \phi \\ f &= 1 \end{aligned} \right\} \text{for } \begin{cases} -\frac{\pi}{2} < \phi < \phi_{\min} \\ \phi_{\min} < \phi < \phi_{\max} \\ \phi_{\max} < \phi < \frac{\pi}{2} \end{cases}$$

We wish to find the average fraction \bar{f} of a beam of width $A \cos \phi$ as ϕ ranges from $-(\pi/2)$ to $(\pi/2)$, given by the expression

$$\begin{aligned} \bar{f} &= \frac{\int_{\phi=-\frac{\pi}{2}}^{\frac{\pi}{2}} A f(\phi) \cos \phi \, d\phi}{\int_{\phi=-\frac{\pi}{2}}^{\frac{\pi}{2}} A \cos \phi \, d\phi} \\ &= \frac{1}{2A} \left[\int_{\phi_{\min}}^{\phi_{\max}} \left(\frac{r_A \sin(\phi - \phi_{\min})}{A \cos \phi} \right) A \cos \phi \, d\phi + \int_{\phi_{\max}}^{\frac{\pi}{2}} A \cos \phi \, d\phi \right] \\ &= \frac{1}{2A} \left[-r_A \cos(\phi_{\max} - \phi_{\min}) + r_A + A - A \sin \phi_{\max} \right] \end{aligned}$$

From the definitions of r_A and r_o , we find $x/r_a = \cos \phi_{\min}$, $x/r_o = \cos \phi_{\max}$, $y/r_o = \sin \phi_{\max}$, $(y - A)/r_A = \sin \phi_{\min}$, so

$$\begin{aligned}
\bar{f} &= \frac{1}{2A} \left[r_A (1 - \cos \phi_{\max} \cos \phi_{\min} - \sin \phi_{\max} \sin \phi_{\min}) \right. \\
&\quad \left. + A (1 - \sin \phi_{\max}) \right] \\
&= \frac{1}{2A} \left[r_A \left(1 - \frac{x^2}{r_o r_A} - \frac{y^2 - Ay}{r_o r_A} \right) + A \left(1 - \frac{y}{r_o} \right) \right] \\
&= \frac{1}{2A} \left[r_A - \frac{x^2 + y^2}{r_o} + A \right] \\
&= \frac{1}{2A} [A - r_o + r_A]
\end{aligned}$$

This is the form derived previously by a quite different approach.

THE CHARACTER OF THE PROBABILITY MATRICES

For the linear two-dimensional arrays, louvre and chevron (Fig. 1), it is plain that the equations for P_{ij} give zero for collinear segment probabilities. The matrix will thus always be zero on the principal diagonal and for groups (minors) in any one face. Other zeroes may occur for complete masking.

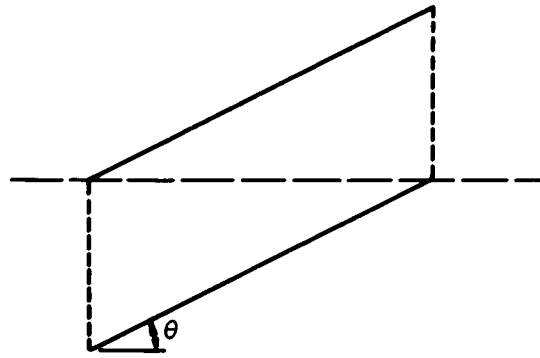
There are also in these configurations symmetrical properties which appear in the matrix if only a symmetrical numbering scheme is used.

We saw previously that the matrix to be inverted (for asymptotic values) is of form

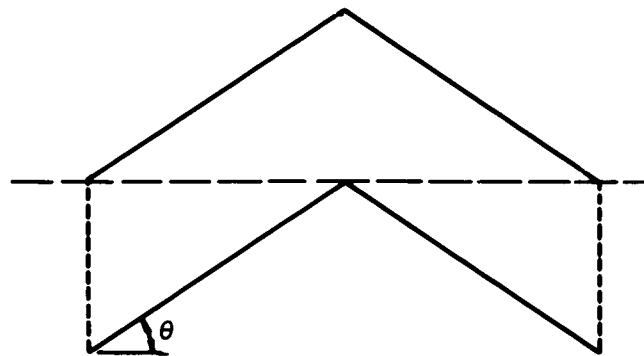
$$\{I - AP'\} \text{ or } \{I - P'A\}$$

which, due to the collinearity mentioned above, is always unity for every main diagonal element. Since we have $0 \leq A_{ij} \leq 1$ and $0 \leq P_{ij} \leq 1$ in all open polygonal configurations, the matrix to be inverted always has a strong "backbone". This explains why matrix inversion works very well even for 48 by 48 matrices and single precision in these problems.

In more general, say three-dimensional cases, the diagonal (P_{ij}) elements will be non-zero if a surface element is actually concave (as within a segment of a sphere). By further subdivision, they may be made quite small, while the $(I - AP')$ or $(I - P'A)$ matrix maintains a strong trace. Thus the only trouble expected from the matrix inversion would occur for extremely numerous divisions; this is round-off error, and even this limitation can be extended by using double precision matrix inversion.



Louvre



Chevron

Fig. 1 Baffle Geometry

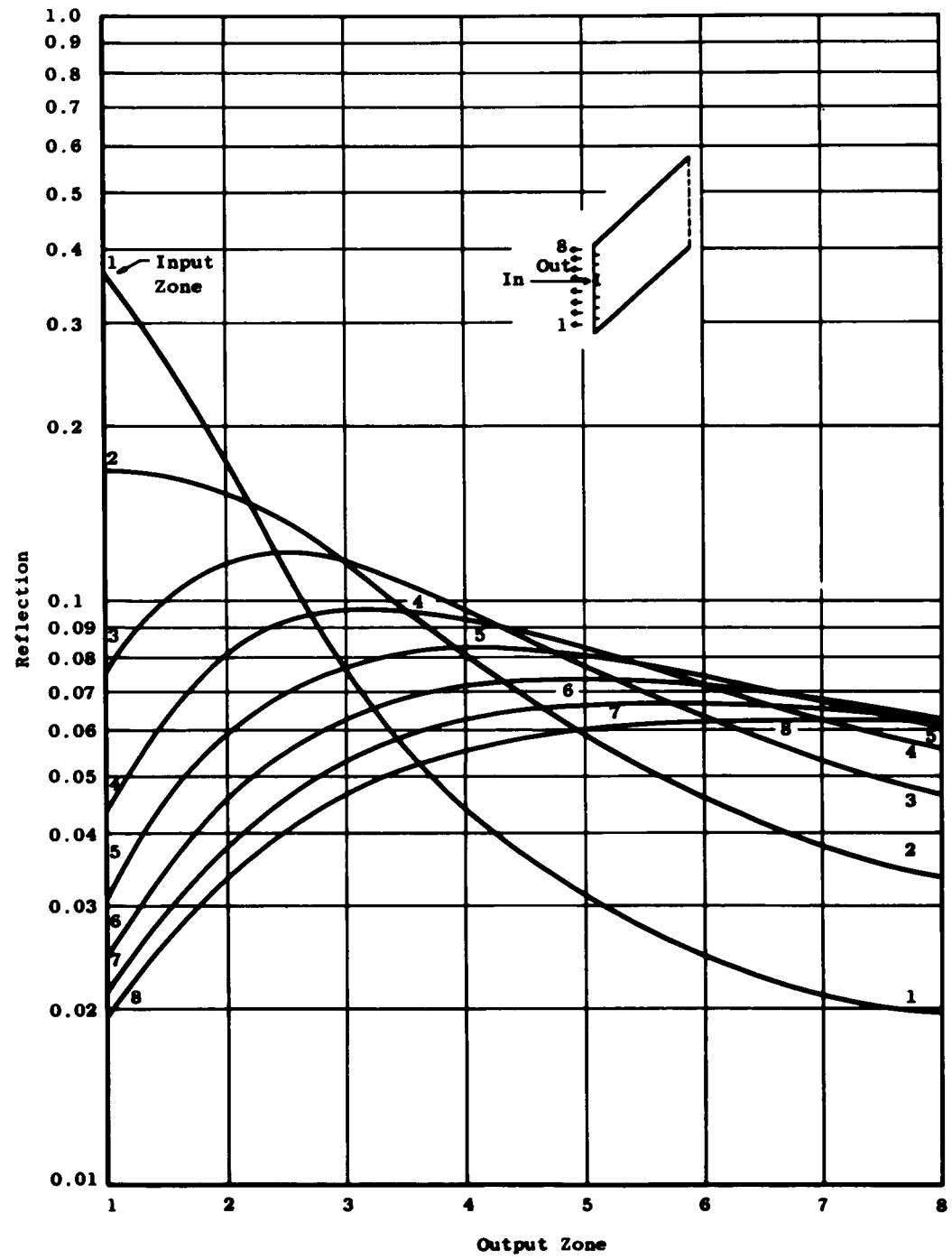


Fig. 2 Reflection Distribution by Zones for Single Zone Input (Louvre)

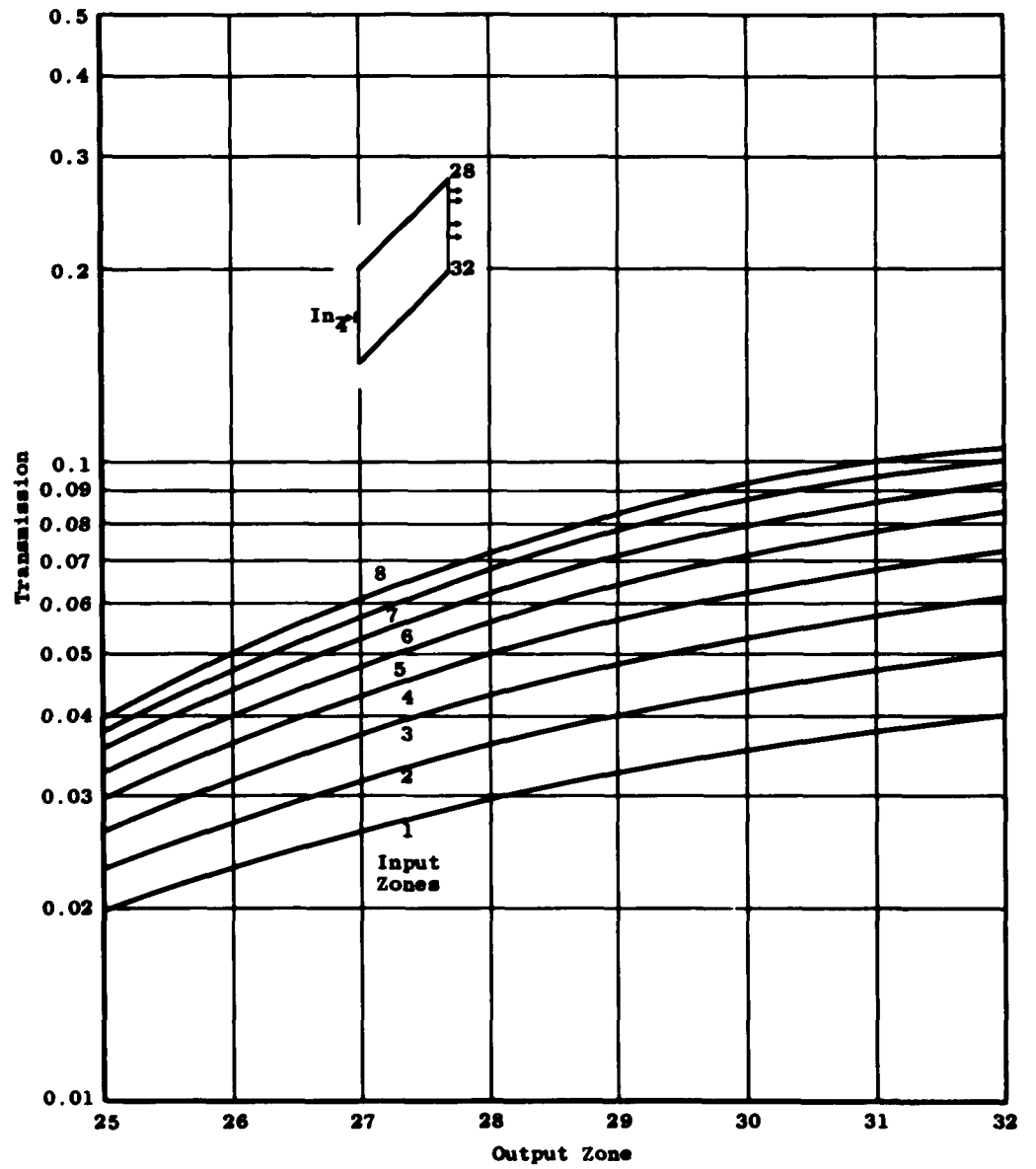


Fig. 3 Transmission Distribution by Zones for Single Zone Input (Louvre)

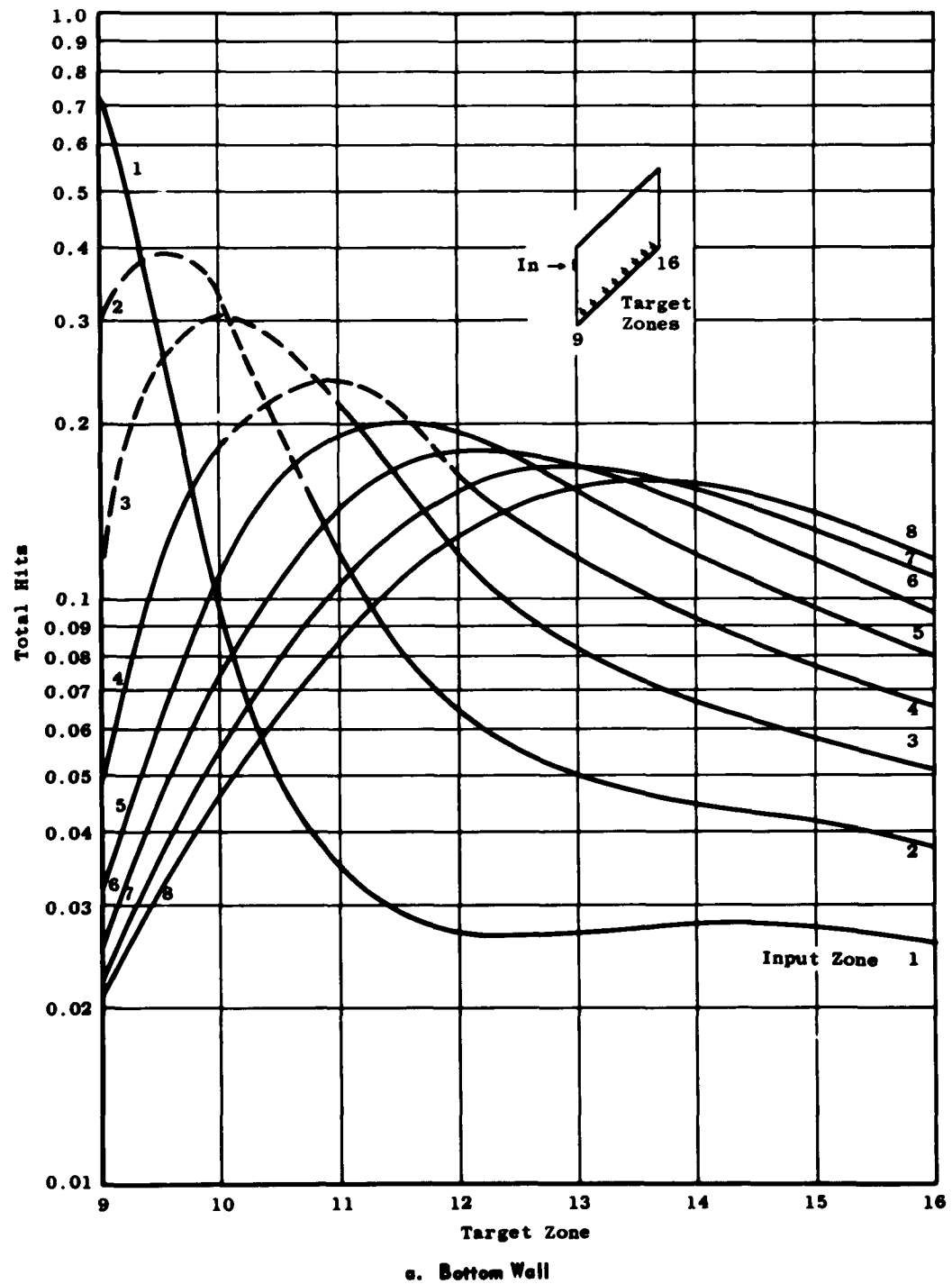
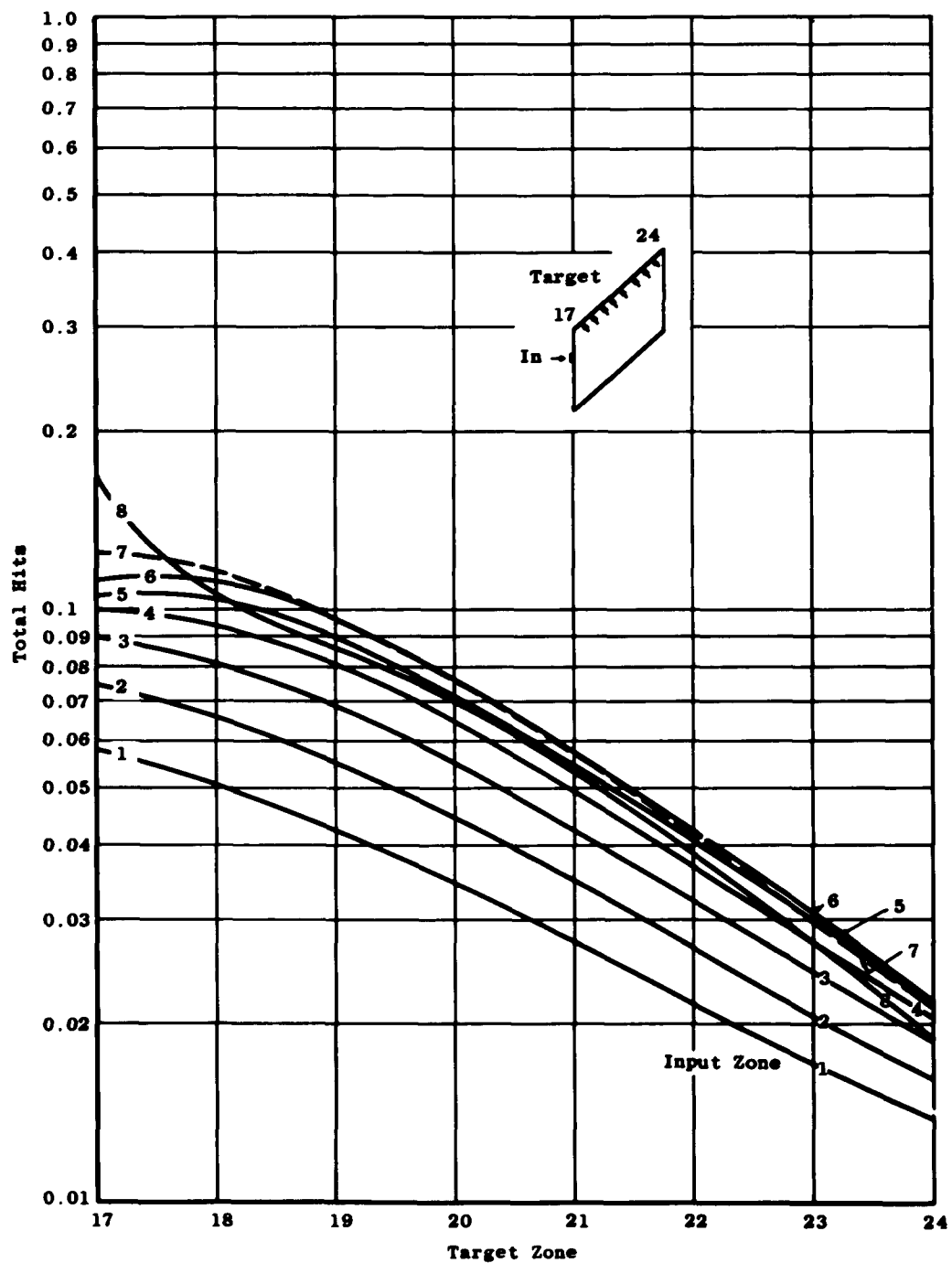


Fig. 4 Total Hit Distributions by Zones for Single Zone Input (Leuvre), $\theta = 45$ deg



b. Top Well

Fig. 4 Concluded

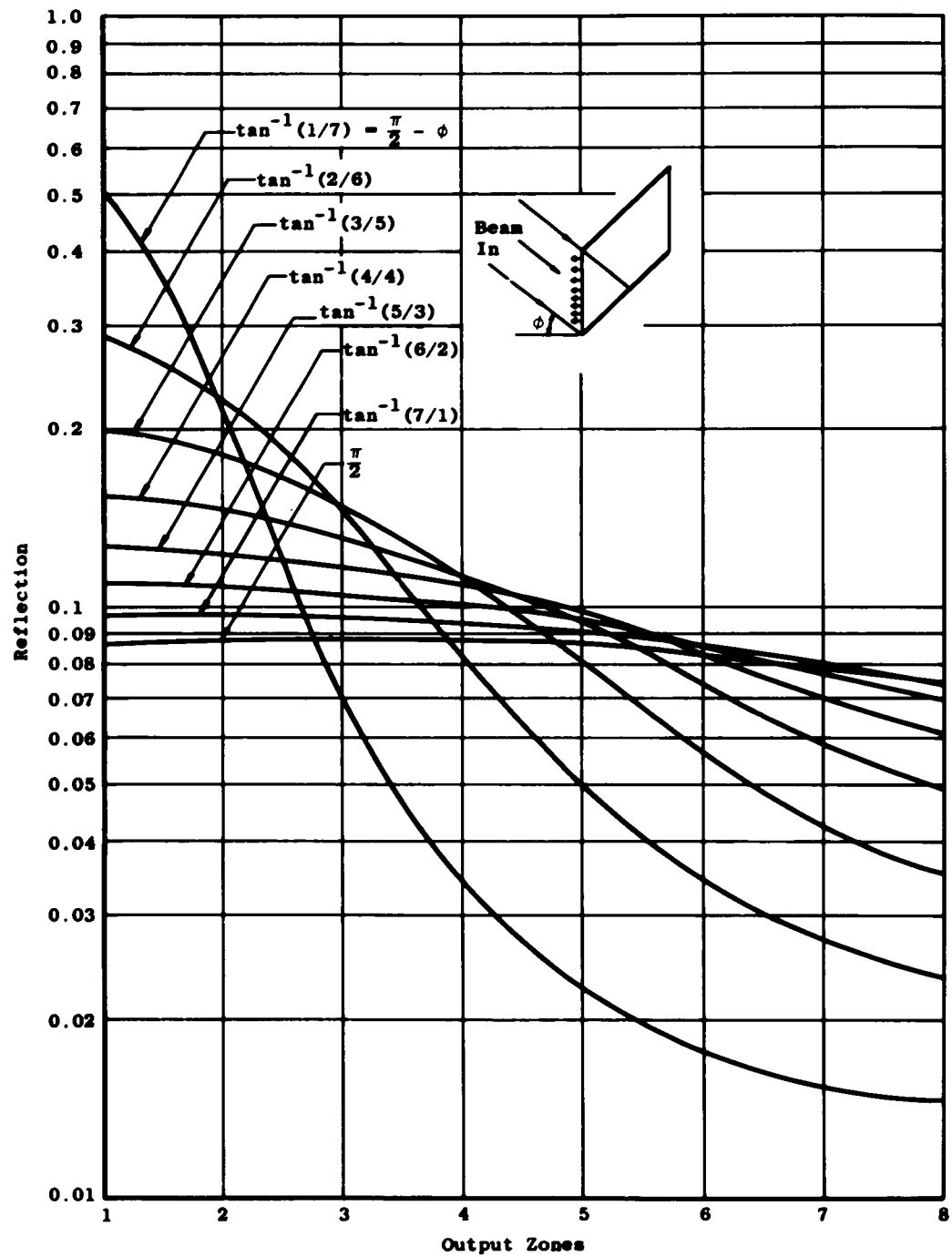
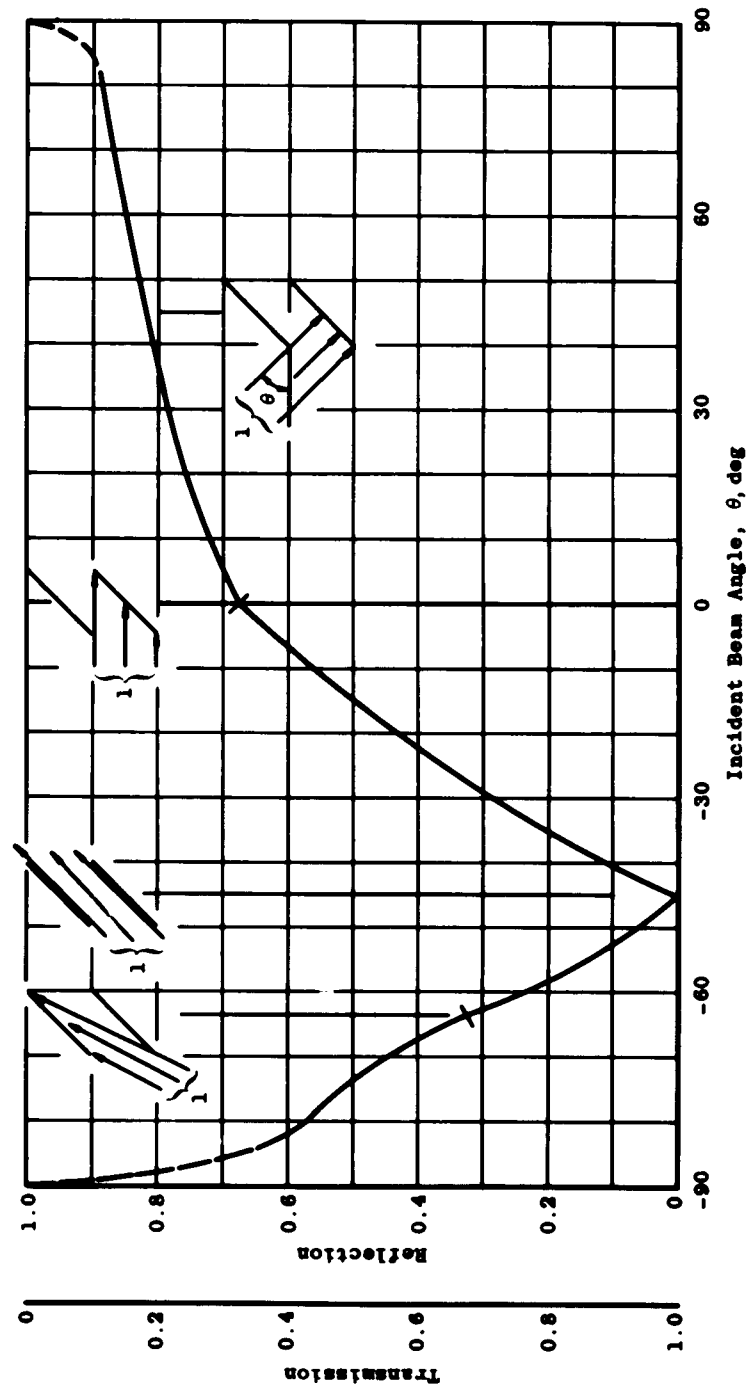
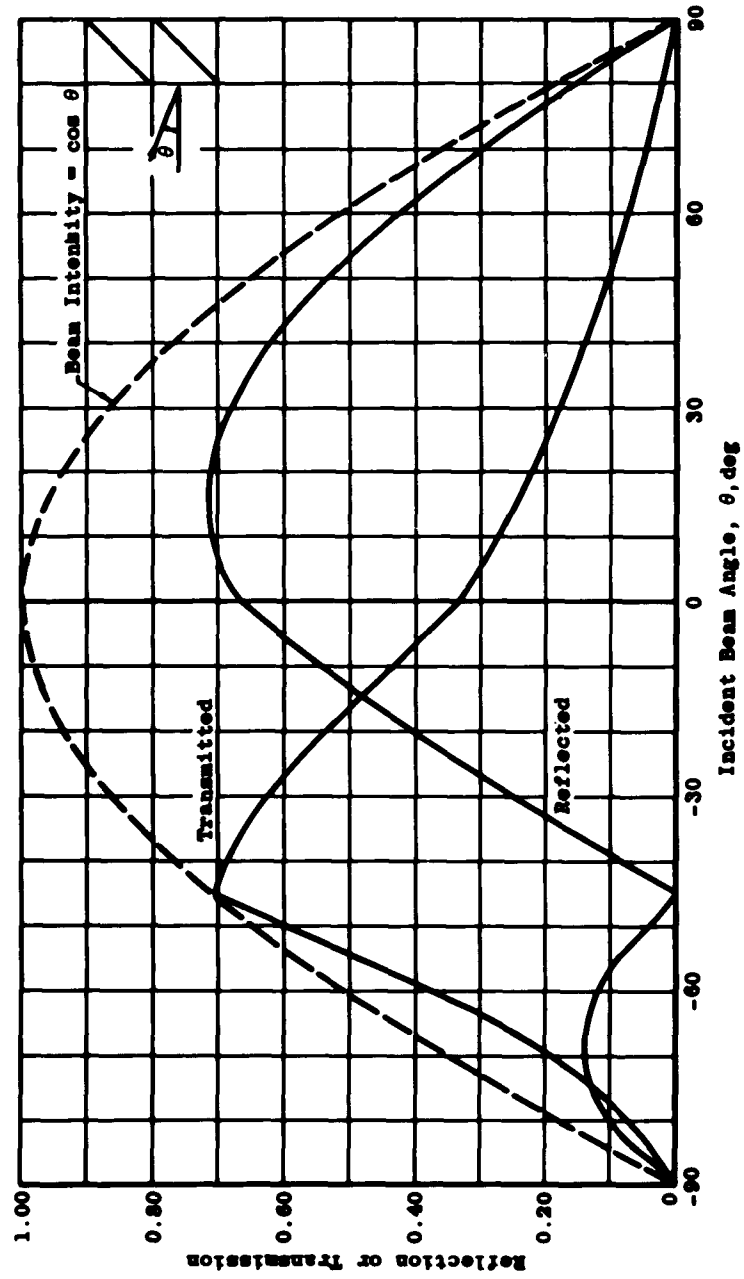


Fig. 5 Reflection by Zones for Directed Beam (Louvre), $\phi = 45$ deg



a. Unit Total Beam Strength
 Fig. 6 Reflection and Transmission of a Directed Beam (Louvre)



b. Finite Entrance
Fig. 6 Concluded

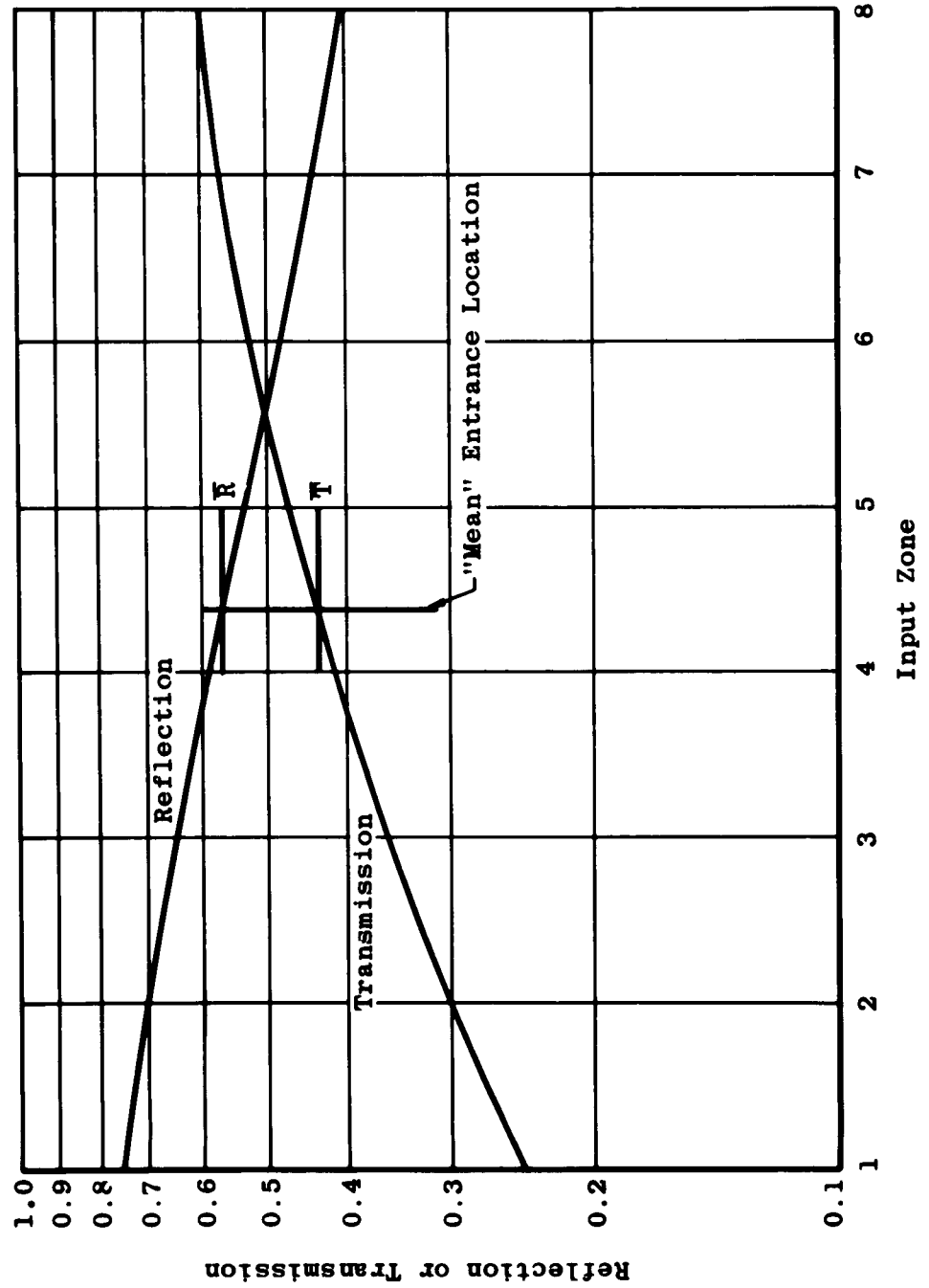
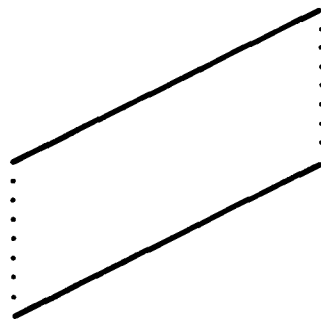
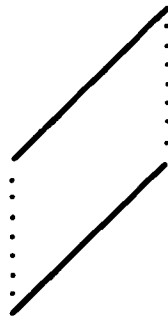
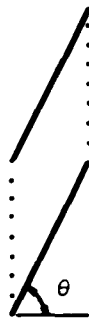


Fig. 7 Total Output for Single Input Zone (Leuvre), $\theta = 45^\circ$



Louvre	$\theta = 30^\circ$	R = 53.7	T = 46.3
	45°	56.7	43.3
	60°	52.8	47.2
Parallel Plates (Faces in Ratio 4:1)		59.6	40.4

Fig. 8 Typical Configurations and Summary of Results

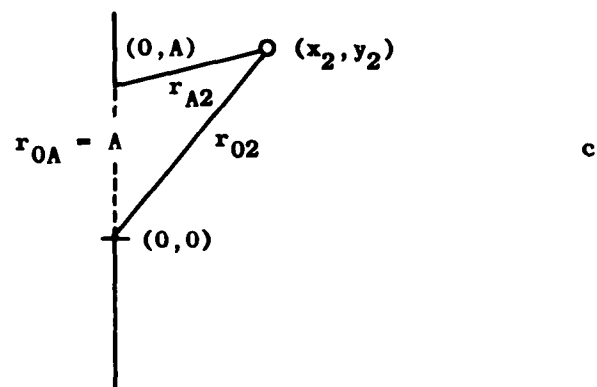
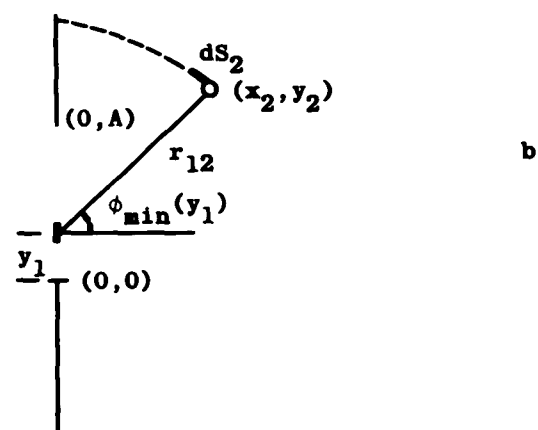
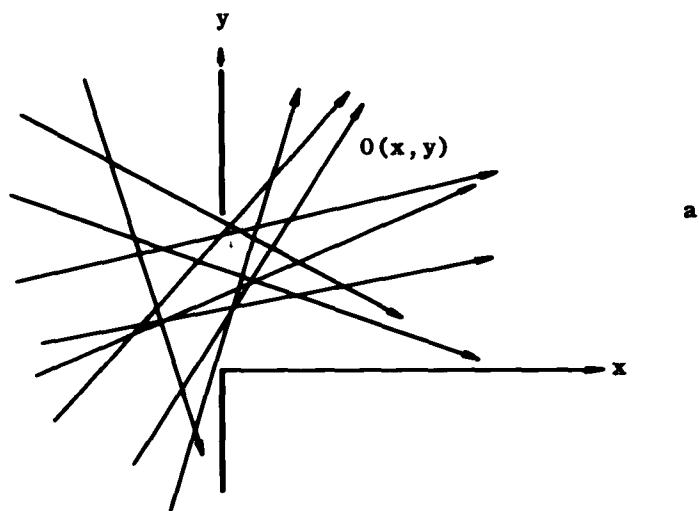


Fig. 9 Random Angle Geometry for Probability Calculations

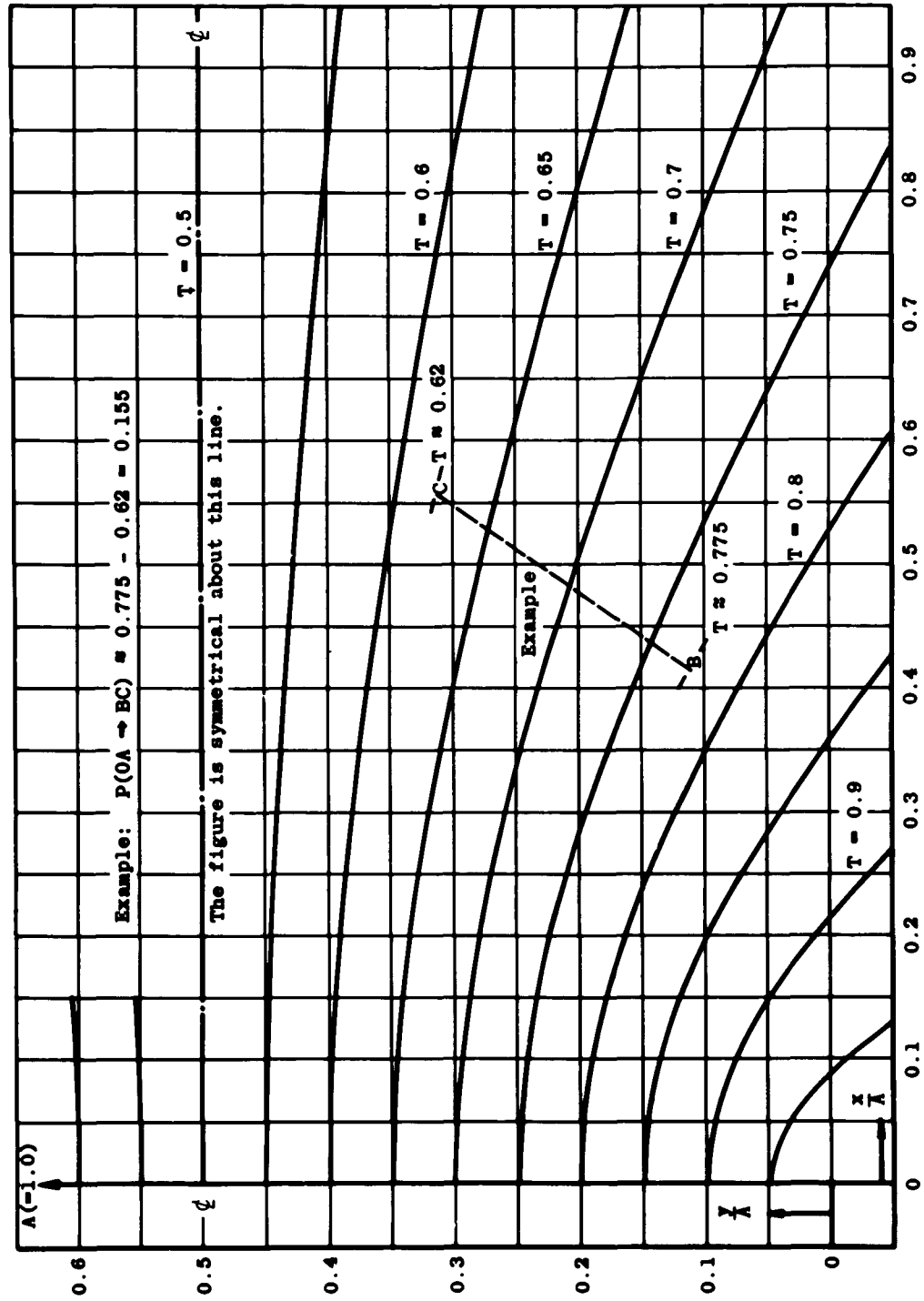
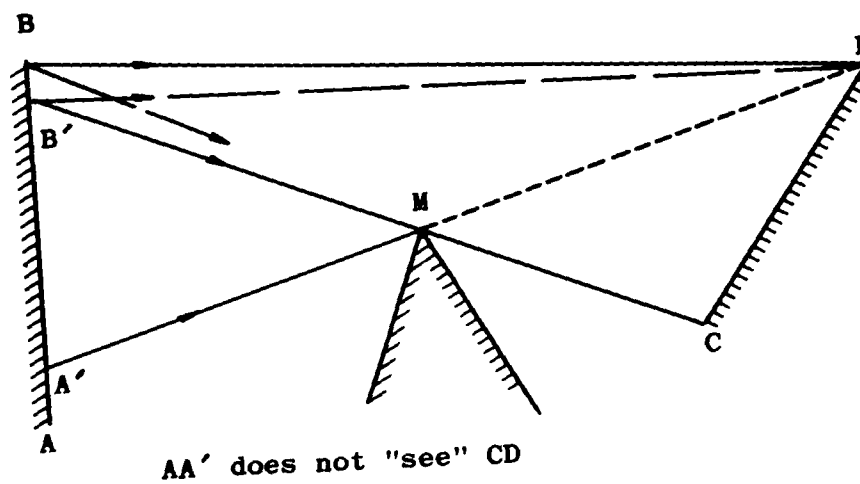
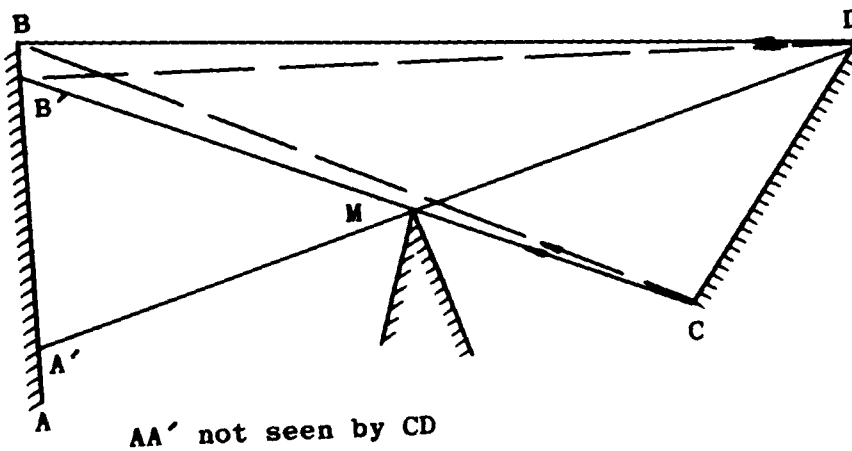


Fig. 10 Curves of Constant Transmission

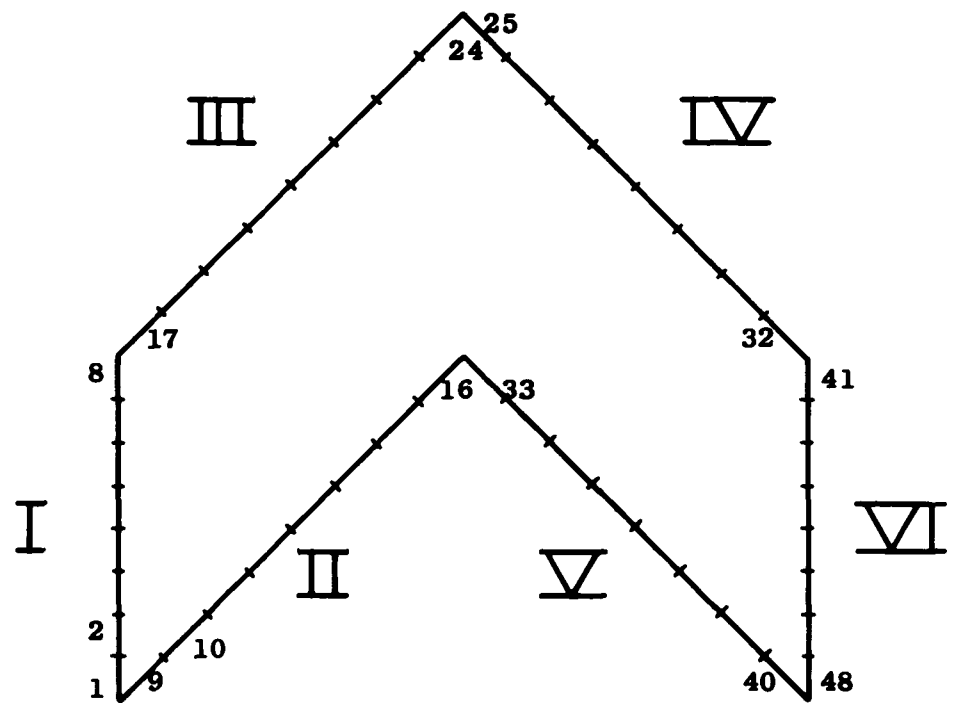


$$P(\overline{AB} \rightarrow \overline{CD}) = \frac{\overline{A'B'}}{\overline{AB}} \times P(\overline{A'B'} \rightarrow \overline{MD}) + \frac{\overline{B'B}}{\overline{AB}} \times P(\overline{B'B} \rightarrow \overline{CD})$$



$$P(\overline{CD} \rightarrow \overline{AB}) = P(\overline{CD} \rightarrow \overline{B'B}) + P(\overline{CD} \rightarrow \overline{MB'})$$

Fig. 12 Masking by Convex Corner



Chevron

Surfaces I and VI are open; all others are solid walls.

Fig. 13 Schematic of Chevron Configuration

θ = Angle defining lower boundary of polar zone
 γ = Arc sin r_v/r_c
 I = Index of source zone
 J = Index of target zone
 Subscript c = "chamber wall", outer sphere
 Subscript v = "vehicle", inner sphere

$$\begin{aligned}
 1. \quad P_{cv}(\theta_I, \theta_J) &= \frac{\sin \theta_J \sin \gamma}{2} - \frac{G\gamma}{2} \\
 2. \quad P_{cv}(\theta_I, \theta_J) &= \frac{\sin \theta_J \sin \gamma}{2\gamma} \phi_o + \frac{\sin^2 \gamma}{\gamma} \left(\frac{\gamma}{2} - \beta_o \right) - G \tan^{-1} \left[X_1 \left(\frac{\lambda-1}{\lambda+1} \right)^{1/2} \right] \\
 \phi_o &= \cos^{-1} \left[\frac{\sin \gamma - \sin \theta_I \sin \theta_J}{\cos \theta_I \cos \theta_J} \right] \\
 \beta_o &= \sin^{-1} \left[\frac{\sin \theta_J - \sin \gamma \sin \theta_I}{\cos \gamma \cos \theta_I} \right] \\
 G &= \frac{\sin \gamma \left[(1 + \sin^2 \gamma) \sin \theta_J - 2 \sin \gamma \sin \theta_I \right]}{\gamma \left\{ [2 \sin \gamma \cos(\theta_I + \theta_J) + 1 + \sin^2 \gamma] [-2 \sin \gamma \cos(\theta_I - \theta_J) + 1 + \sin^2 \gamma] \right\}^{1/2}} \\
 X_1 &= \left[\frac{\cos(\theta_I - \theta_J) - \sin \gamma}{\cos(\theta_I + \theta_J) + \sin \gamma} \right]^{1/2} \\
 \frac{\lambda-1}{\lambda+1} &= \frac{2 \sin \gamma \cos(\theta_I + \theta_J) + 1 + \sin^2 \gamma}{-2 \sin \gamma \cos(\theta_I - \theta_J) + 1 + \sin^2 \gamma} \\
 3. \quad P_{vc}(\theta_I, \theta_J) &= \frac{\sin \theta_J}{2 \sin \gamma} - \frac{\gamma G}{2 \sin^2 \gamma} \\
 4. \quad P_{vc}(\theta_I, \theta_J) &= \frac{\sin \theta_J}{2\gamma \sin \gamma} \phi_o + \frac{1}{\gamma} \left(\frac{\gamma}{2} - \beta_o \right) - \frac{G}{\sin^2 \gamma} \tan^{-1} \left[X_1 \left(\frac{\lambda-1}{\lambda+1} \right)^{1/2} \right] \\
 (\phi_o, \beta_o, G, X_1, \frac{\lambda-1}{\lambda+1}) &\text{ defined above} \\
 5. \quad P_{cc}(\theta_I, \theta_J) &= -\frac{\sin \theta_I}{2} + \frac{1}{2} \\
 6. \quad P_{cc}(\theta_I, \theta_J) &= -\frac{\sin \theta_J}{2} + \frac{1}{2} - \sin^2 \gamma \\
 7. \quad P_{cc}(\theta_I, \theta_J) &= -\frac{\sin \theta_I}{2\gamma} \phi_o + \frac{1}{\gamma} \left(\frac{\gamma}{2} - \beta_o \right) \cos^2 \gamma + \frac{1}{\gamma} \tan^{-1} \left[X_1 \left(\frac{\lambda-1}{\lambda+1} \right)^{1/2} \right] \\
 \phi_o &= \cos^{-1} \left[-\frac{\cos 2\gamma + \sin \theta_I \sin \theta_J}{\cos \theta_I \cos \theta_J} \right] \\
 \beta_o &= \sin^{-1} \left[\cot 2\gamma \tan \theta_I + \frac{\sin \theta_J}{\sin 2\gamma \cos \theta_I} \right] \\
 X_1 &= \left[\frac{\cos(\theta_I - \theta_J) + \cos 2\gamma}{\cos(\theta_I + \theta_J) - \cos 2\gamma} \right]^{1/2} \\
 \left(\frac{\lambda-1}{\lambda+1} \right)^{1/2} &= \frac{1 - \cos(\theta_I + \theta_J)}{\sin \theta_I + \sin \theta_J}
 \end{aligned}$$

Fig. 14 Probability Equations of Concentric Spheres



$\gamma = 75^\circ$
 No Pumping
 Unit Input on Equatorial
 Zones 18, 19 Both Spheres

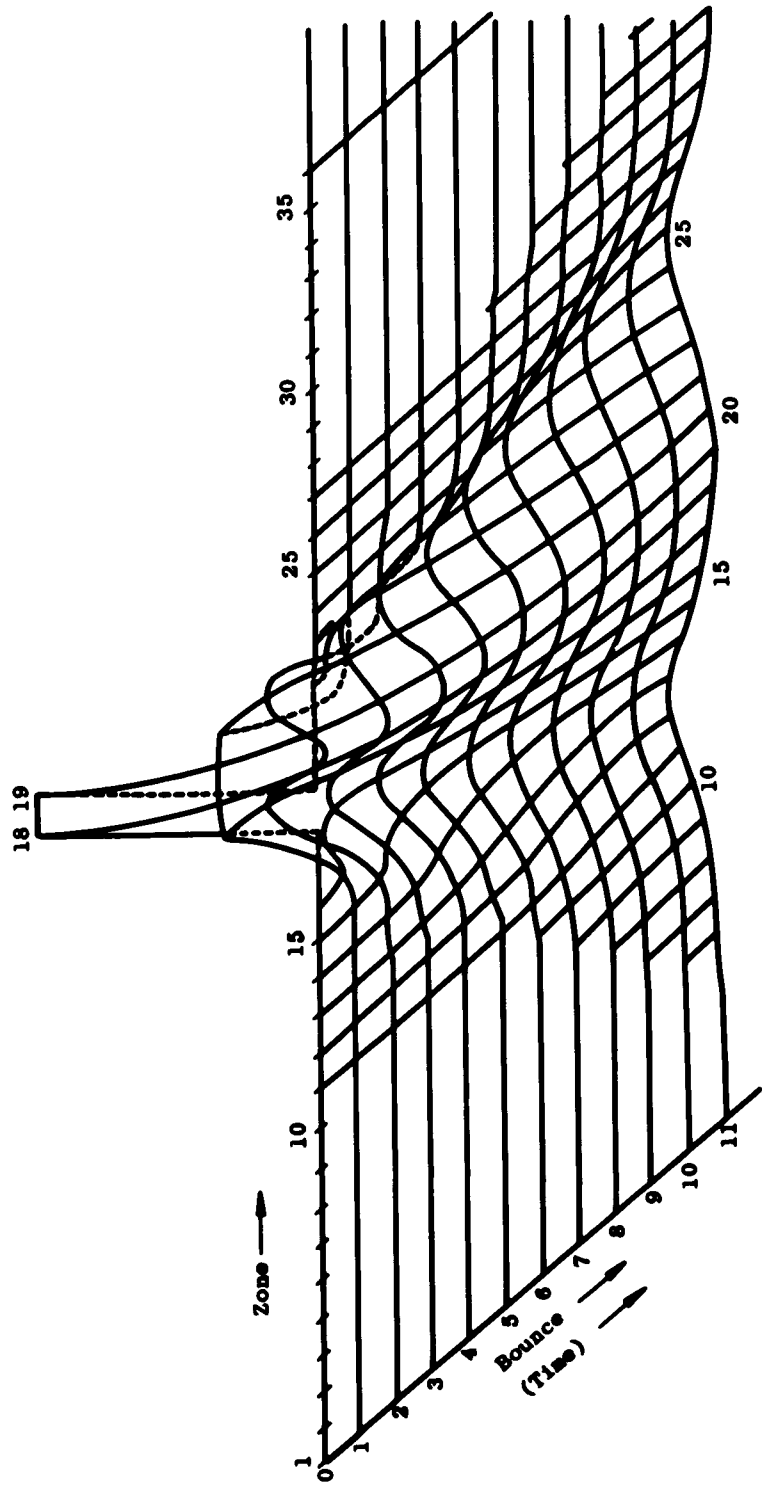
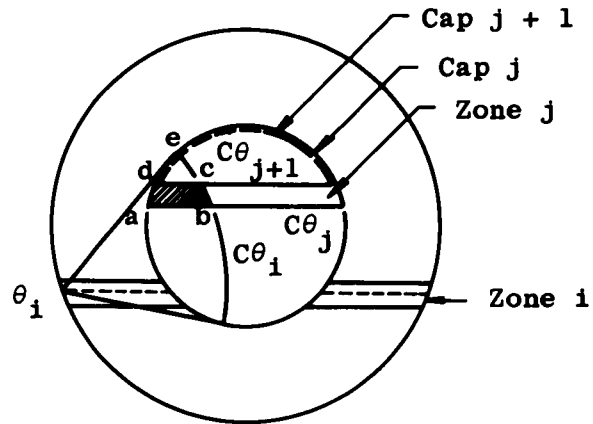


Fig. 15 Pulse Propagation between Concentric Spheres



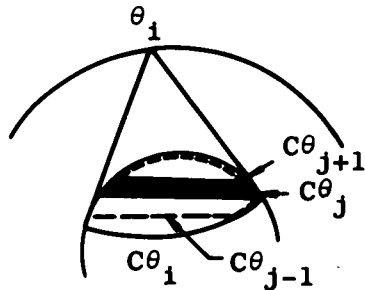
To find $P(\theta_i, \theta_j)$, probability for transfer from zone i to zone j, find first for "caps"

$$P(\theta_i, \theta > \theta_j)$$

Then $P(\theta_i, \theta > \theta_{j+1})$

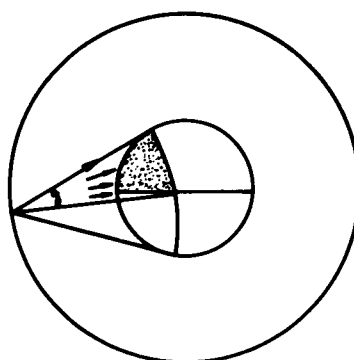
and $P(\theta_i, \theta_j) = P(\theta_i, \theta > \theta_j) - P(\theta_i, \theta > \theta_{j+1})$, for zone j

For either $P(\theta_i, \theta > \theta_j)$ and $P(\theta_i, \theta > \theta_{j+1})$ the boundary arcs are $C\theta_i$ and $C\theta_j$ or $C\theta_{j+1}$.

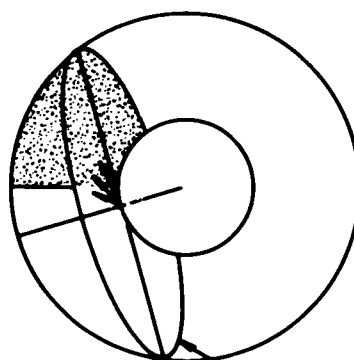


At left the "caps" bounded by $C\theta_j$ and $C\theta_{j+1}$ are bounded by these arcs alone, but the arcs $C\theta_{j-1}$ and $C\theta_i$ are both involved for lower zones.

Fig. 16 Zone Geometry, Concentric Spheres

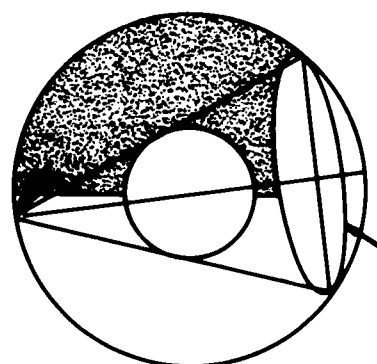


Chamber Wall
to Vehicle



Vehicle to
Chamber Wall

Horizon Plane

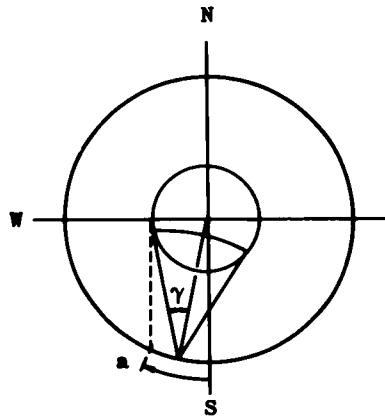


Chamber Wall to
Chamber Wall

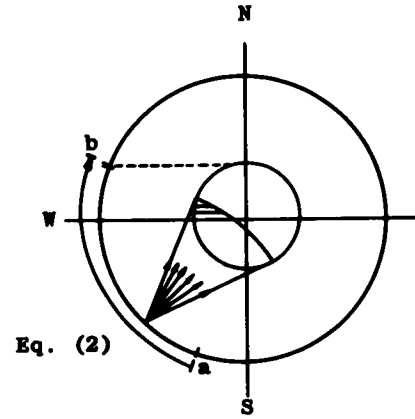
Shadow of
Vehicle

Fig. 17 Molecular Transfers (Target in Northern Hemisphere)

Chamber to Vehicle, $\gamma < \frac{\pi}{4}$

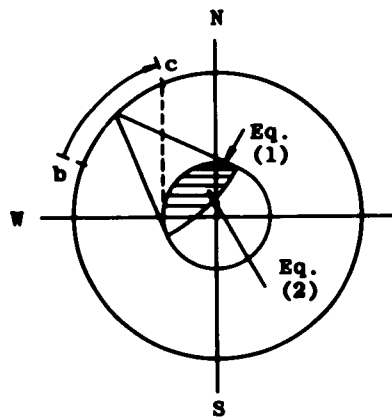


I No transfer to northern hemisphere until a reached.

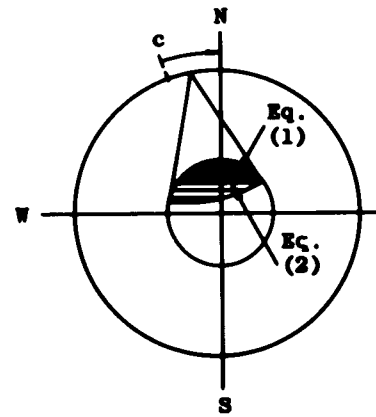


II Transfer to northern hemisphere areas bounded by 2 arcs until point b.

Note: As $\gamma \rightarrow \frac{\pi}{4}$ point b and c merge; type III does not occur for $\gamma > \frac{\pi}{4}$. Equations refer to equations in Fig. 14.



III Areas bounded by single arc mixed with 2 arc bound areas.

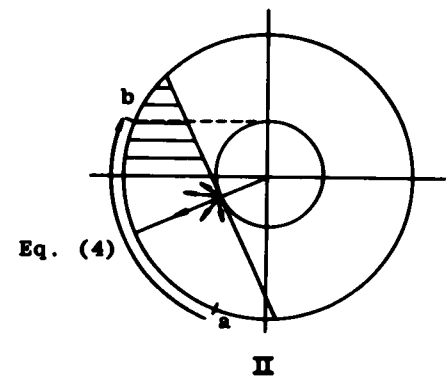
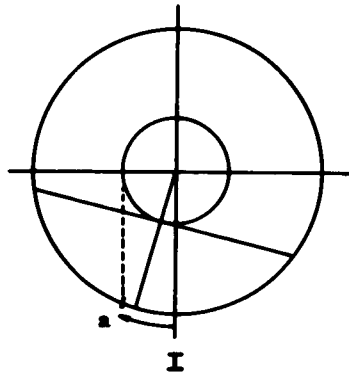


IV No transfer to southern hemisphere after point c.

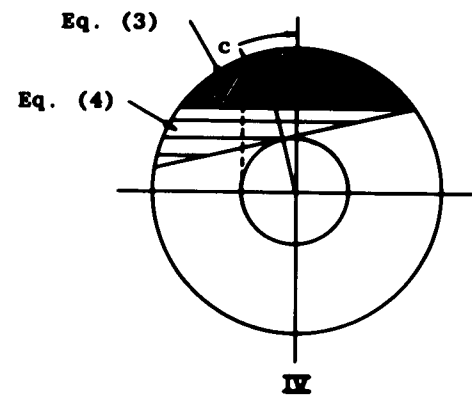
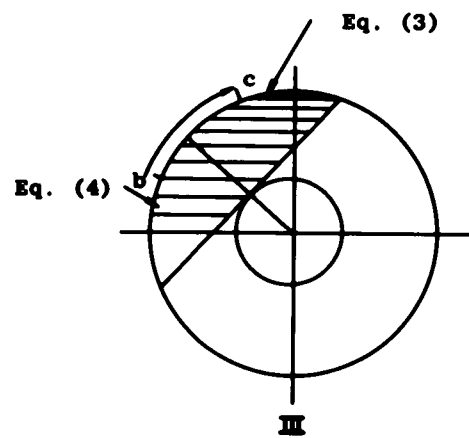
a. Outer Sphere to Inner Sphere

Fig. 18 Types of Transfers

Vehicle to Chamber, $\gamma < \frac{\pi}{4}$



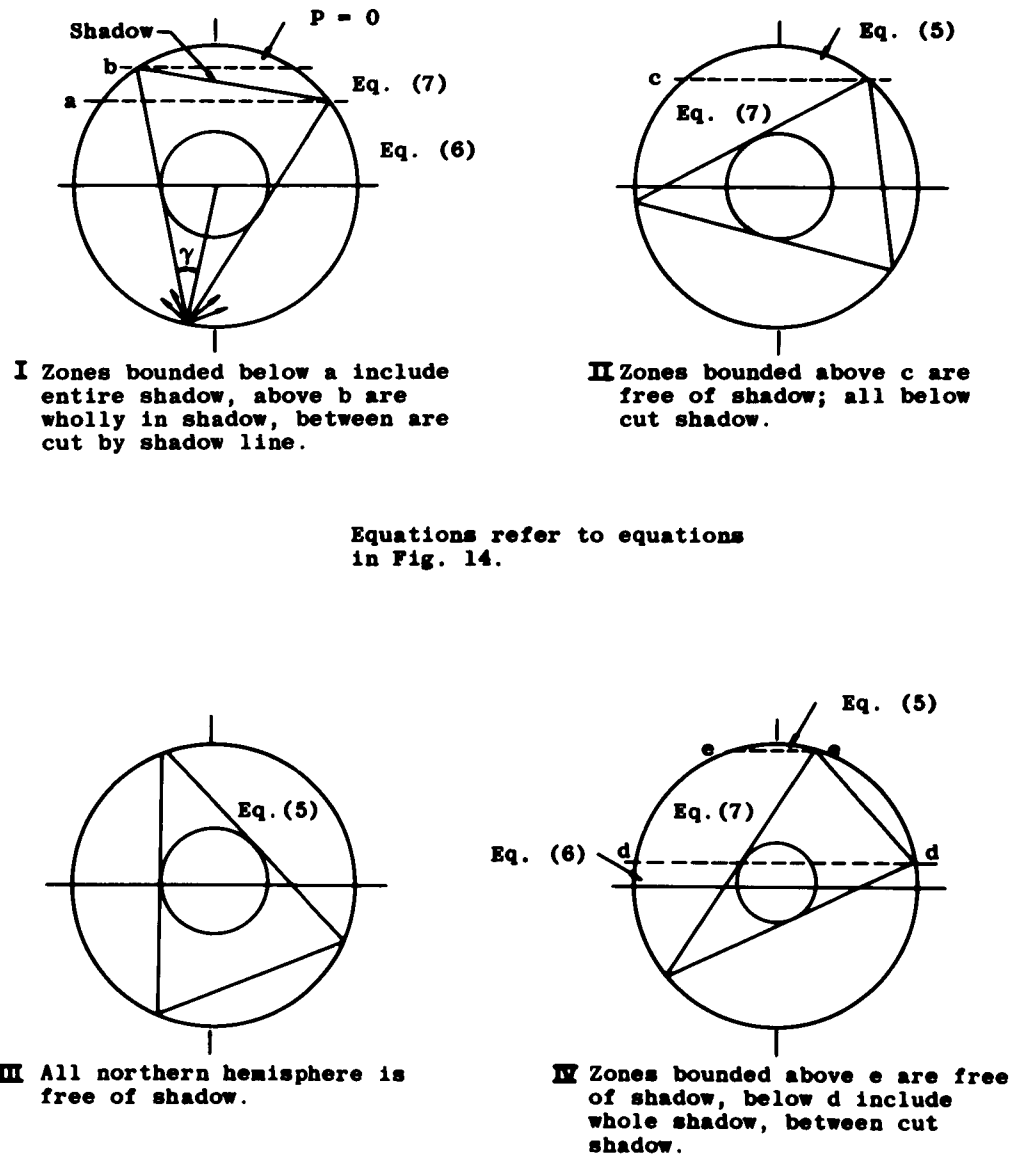
Same commentary holds
for chamber to vehicle
transfers. Equations
refer to equations in
Fig. 14.



b. Inner Sphere to Outer Sphere

Fig. 18 Continued

Chamber to Chamber



c. Outer Sphere to Outer Sphere

Fig. 18 Concluded

